JGR Space Physics

RESEARCH ARTICLE
10.1029/2021JA029188

**Key Points:**

- A statistical study of $B_Z$ in jets is conducted using Time History of Events and Macroscale Interactions during Substorms 2008–2011 data from the subsolar magnetosheath
- 60-70% of jet intervals contain a pulse of $B_Z$ opposite to the interplanetary magnetic field $B_Z$ while majority of non-jet intervals do not
- The median duration of the longest opposite $B_Z$ burst in jets is ~10s and strength is ~±10nT

**Supporting Information:**

Supporting Information may be found in the online version of this article.

**Correspondence to:**

L. Vuorinen,
lakavu@utu.fi

**Citation:**

Vuorinen, L., Hietala, H., Plaschke, F., & LaMoury, A. T. (2021). Magnetic field in magnetosheath jets: A statistical study of $B_Z$ near the magnetopause. *Journal of Geophysical Research: Space Physics*, *126*, e2021JA029188. https://doi.org/10.1029/2021JA029188

Received 27 JAN 2021
Accepted 12 AUG 2021



# Magnetic Field in Magnetosheath Jets: A Statistical Study of $B_Z$ Near the Magnetopause

**Laura Vuorinen[1], Heli Hietala[1,2,3], Ferdinand Plaschke[4], and Adrian T. LaMoury[2]**

[1]Department of Physics and Astronomy, University of Turku, Turku, Finland, [2]Blackett Laboratory, Imperial College London, London, UK, [3]Department of Earth, Planetary, and Space Sciences, University of California, Los Angeles, CA, USA, [4]Space Research Institute, Austrian Academy of Sciences, Graz, Austria

**Abstract** Magnetosheath jets travel from the bow shock toward the magnetopause, and some of them eventually impact it. Jet impacts have recently been linked to triggering magnetopause reconnection in case studies by Hietala et al. (2018, https://doi.org/10.1002/2017gl076525) and Nykyri et al. (2019, https://doi.org/10.1029/2018ja026357). In this study, we focus on the enhancing or suppressing effect jets could have on reconnection by locally altering the magnetic shear via their own magnetic fields. Using observations from the years 2008–2011 made by the Time History of Events and Macroscale Interactions during Substorms spacecraft and solar wind OMNI data, we statistically study for the first time $B_Z$ within jets in the Geocentric Solar Magnetospheric coordinates. We find that $B_Z$ opposite to the prevailing interplanetary magnetic field (IMF) $B_Z$ is roughly as common in jets as in the non-jet magnetosheath near the magnetopause, but these observations are distributed differently. 60–70% of jet intervals contain bursts of opposite polarity $B_Z$ in comparison to around 40% of similar non-jet intervals. The median duration of such a burst in jets is 10 s and strength is ±10nT. We also investigate the prevalence of the type of strong $B_Z \leq -24$nT pulses that Nykyri et al. (2019, https://doi.org/10.1029/2018ja026357) linked to a substorm onset. In our data set, such pulses were observed in around 13% of jets. Our statistical results indicate that jets may have the potential to affect local magnetopause reconnection via their magnetic fields. Future studies are needed to determine whether such effects can be observed.

**Plain Language Summary** Fast earthward flows called jets are often observed within the magnetosheath. They form at the Earth's bow shock, where the solar wind is slowed down before diverting around the magnetosphere. These jets may hit the boundary of the magnetosphere, the magnetopause, with high dynamic pressure. Such impacts have been observed to trigger magnetic reconnection, in which the interplanetary magnetic field (IMF) of the solar wind connects with the Earth's magnetic field and solar wind can enter the magnetosphere. Magnetopause reconnection usually occurs when the IMF points southward, opposite to the Earth's northward field. However, jets have been proposed to trigger reconnection also during northward IMF. We study the magnetic field within jets using data from the Time History of Events and Macroscale Interactions during Substorms spacecraft and solar wind OMNI data from 2008–2011. We find that it is statistically more likely for a magnetosheath interval, associated with jet conditions, to exhibit short pulses of magnetic field directed opposite to the upstream IMF, than for a non-jet interval of the same duration. Therefore, jets may have the potential to affect local reconnection at the magnetopause. Our results motivate future studies that investigate these possible jet-related effects on reconnection.

## 1. Introduction

The dynamics of the Earth's magnetosphere depend greatly on the orientation of the interplanetary magnetic field (IMF) that is carried by the solar wind. This orientation determines the global structure of the bow shock (BS) by controlling the locations of the quasi-parallel ($\theta_{Bn} < 45°$) and quasi-perpendicular ($\theta_{Bn} > 45°$) shock regions. The turbulent foreshock region that forms upstream of the quasi-parallel shock due to the interaction of shock-reflected particles and the incoming solar wind is full of ultralow frequency (ULF) waves (Burgess & Scholer, 2015). The steepening of ULF waves can lead to short large amplitude magnetic structures (SLAMS) that advect toward the bow shock (Schwartz, 1991). These structures are believed to contribute to the observed rippled structure of the quasi-parallel shock surface (Lucek et al., 2008).

Because the IMF is convected into the magnetosheath with the shocked solar wind, the IMF orientation also largely determines the underlying magnetic field structure of the turbulent magnetosheath (Fairfield, 1967; Spreiter et al., 1966). As the plasma flows around the magnetosphere, the field lines are draped around the magnetopause (MP), becoming tangential to it. Depending on local plasma parameters and most importantly the magnetic shear angle between the magnetosheath magnetic field on one side of the magnetopause and the magnetospheric field on the other side, the magnetosheath field either piles up at the magnetopause or reconnects with the Earth's magnetic field. Magnetopause reconnection allows for solar wind energy and plasma to enter the magnetosphere, and can be arguably called one of the most important space weather processes. At the subsolar magnetopause, where the Earth's magnetic field is northward, this process is efficiently driven when the IMF is southward (e.g., Cassak & Fuselier, 2016). Conversely, a magnetic pile-up layer forms in front of the subsolar magnetopause during northward IMF (Phan et al., 1994).

Magnetosheath jets are localized plasma regions that exhibit higher dynamic pressure than the surrounding magnetosheath plasma (Plaschke et al., 2018, and the references therein). Previous studies (e.g., Archer & Horbury, 2013; Plaschke et al., 2013) have reported that these jets are more commonly observed closer to the bow shock than close to the magnetopause, and they mostly occur during intervals of low IMF cone angle (the acute angle between the Sun-Earth line and the IMF). According to Vuorinen et al. (2019), jets are observed nine times more often downstream of the quasi-parallel shock than the quasi-perpendicular shock. Hietala et al. (2009) proposed that the formation of magnetosheath jets could be linked to the rippled nature of the quasi-parallel shock: jets could form due to solar wind flow through a shock ripple. Other suggested mechanisms that could explain the formation of some jets are, for example, SLAMS penetrating into the magnetosheath (Karlsson et al., 2015) and solar wind discontinuities (Archer & Horbury, 2013). In a recent statistical study, Raptis et al. (2020) used MMS data to investigate and classify jets and found both the ripple and SLAMS formation mechanisms to be supported by the data. They also suggested that the impact of IMF on jet formation and properties may be larger than has been thought. A recent 3D hybrid simulation study by Omelchenko et al. (2021) supports this notion, as they linked the formation of jets to entangled field-lines turbulently convecting in the magnetosheath, facilitating compression of solar wind plasma into jets.

Some of these jets can make it to the magnetopause, and their high-dynamic pressure impacts on this boundary have been observed to cause many types of effects. Examples include magnetopause surface waves, which in the event studied by Archer et al. (2019) enabled the first ever direct observation of the magnetopause eigenmode, and ionospheric responses such as aurorae (Wang et al., 2018). These observed effects highlight the role of jets in bringing solar wind energy into the magnetosphere. Importantly, magnetosheath jets are not a rare phenomenon, and jets are estimated to be frequently impacting the magnetopause (Plaschke et al., 2016; Plaschke, Hietala, & Vörös, 2020). For instance, large jets with diameters $>1R_E$ have estimated impact rates of 5–60 jets per hour on the subsolar magnetopause from high to low IMF cone angle conditions (Vuorinen et al., 2019).

Recently jets have been discussed and studied in the context of magnetopause reconnection. Magnetosheath jets could in principle affect reconnection via multiple ways by changing the local magnetic field and plasma conditions at the magnetopause (as also discussed by Hietala et al., 2018). Some observational evidence has already been provided for two such mechanisms. First, Hietala et al. (2018) observed an event where the magnetopause was unusually thick and the compression by the high-dynamic pressure jet made it thinner until reconnection took place. Second, Nykyri et al. (2019) reported an event where jets drove southward fields toward the magnetopause during northward IMF. Using multi-point observations and timing analysis, they proposed that the jets most likely triggered magnetopause reconnection that then introduced enough magnetic flux to the magnetotail, leading to a substorm onset. As the magnetic shear angle can be regarded as the most important parameter for reconnection, the first step toward understanding how likely it is for jets to statistically affect reconnection is to determine the typical magnetic field $B_Z$ orientation within jet intervals near the magnetopause. This is the aim of this study. Whether jets can be expected to trigger local magnetopause reconnection during northward IMF is of particular interest.

We statistically investigate the magnetosheath magnetic field component $B_Z$, in Geocentric Solar Magnetospheric (GSM) coordinates, to find whether the distribution of $B_Z$ observations in jets is different from the distribution within similar-duration intervals in the non-jet magnetosheath. We study jet intervals and sampled non-jet magnetosheath intervals that have been observed during similar IMF conditions and at

similar locations in the magnetosheath. The data are divided into two categories based on prevailing IMF conditions: northward and southward IMF. Then the data are studied as a function of relative radial position in the magnetosheath and as a function of IMF cone angle close to the magnetopause. This includes studying the general distributions of $B_Z$ in all the intervals, $B_Z$ minima and maxima within the intervals, and durations of southward and northward periods within the intervals.

The study is organized as follows. First, we introduce the data and methods used to study jets and non-jet magnetosheath intervals at varying locations in the magnetosheath. Second, we present the results of our statistical study, after which we discuss the implications and possible explanations of these results, and give our suggestions for future studies. Finally, we summarize and provide the conclusions of this study.

## 2. Data and Methods

We use the jet data set introduced by Plaschke et al. (2013) that consists of Time History of Events and Macroscale Interactions during Substorms (THEMIS) spacecraft (Angelopoulos, 2008) data from 2008 to 2011. We refer the reader to Plaschke et al. (2013) for a complete description. The data set can also be found online (Plaschke, Hietala, & Angelopoulos, 2020). It contains magnetosheath observations from the subsolar region defined by a 30° solar zenith angle and by a radius of 7–18$R_E$ from the center of the Earth. We use measurements from the Fluxgate Magnetometer (FGM) (Auster et al., 2008) and the Electrostatic Analyzer (ESA) (McFadden et al., 2008) that have been interpolated to a 1-s cadence timeline that is shared between the different measurements. The corresponding upstream IMF and solar wind conditions have been obtained from high-resolution OMNI data (King & Papitashvili, 2005; Papitashvili & King, 2020) as running averages of the preceding 5 min.

In total, the data set contains 2,736.9 h of magnetosheath data with 2,859 jets. These jet intervals are comprised of 125,897 1-s data points in total, and they have been selected by the following main criteria (see the original paper by Plaschke et al., 2013 for the total list): (a) at some point within the jet the earthward ($-X$ direction in GSM coordinates) dynamic pressure within a jet has to exceed half of the solar wind dynamic pressure, and (b) within the whole jet interval it has to be larger than a quarter of the solar wind dynamic pressure. This Plaschke et al. (2013) data set suits our purposes well, as we are particularly interested in dynamic pressure enhancements that are headed toward the Earth, can impact the subsolar magnetopause, and affect magnetopause reconnection.

In Figure 1, we present three example magnetosheath intervals containing jets, as defined by the Plaschke et al. (2013) selection criteria. The jet intervals are highlighted in purple shading and the dashed vertical line represents $t_0$, the moment of highest ratio between the magnetosheath and the solar wind dynamic pressures within the jet. In addition, the longest northward and southward $B_Z$ periods within the jets are shaded in orange and magenta, respectively. These examples demonstrate that the magnetic field has a different structure from jet to jet. However, all of these jets seem to introduce variations to the magnetosheath, because there are changes in magnetic field components once the jets are observed. Table 1 shows the relevant parameters of the example jets in the context of this study. These parameters will be described later in this section. In Example 1, we can see wave-like structure within the jet. In Example 2, there is a clear magnetic field discontinuity within the jet—most likely a current sheet. Example 3 shows a short-duration jet, which has clear changes in magnetic field components.

The underlying magnetic field structure of the magnetosheath changes from the bow shock to the magnetopause (Fairfield, 1967; Spreiter et al., 1966). Therefore, we need to study $B_Z$ within jets and within non-jet magnetosheath intervals at varying locations in the magnetosheath. Naturally, we are most interested in these distributions close to the magnetopause, where reconnection takes place. However, the positions and shapes of the bow shock and the magnetopause change during varying solar wind and IMF conditions. In order to determine the relative positions of the spacecraft with respect to the bow shock and the magnetopause, we must take these changes into account. We use the magnetopause model introduced by Shue et al. (1998) and the bow shock model by Merka et al. (2005). We normalize the distance between the magnetopause and bow shock models to unity and set the magnetopause to be at $F = 0$ and the bow shock at $F = 1$ (Archer & Horbury, 2013):

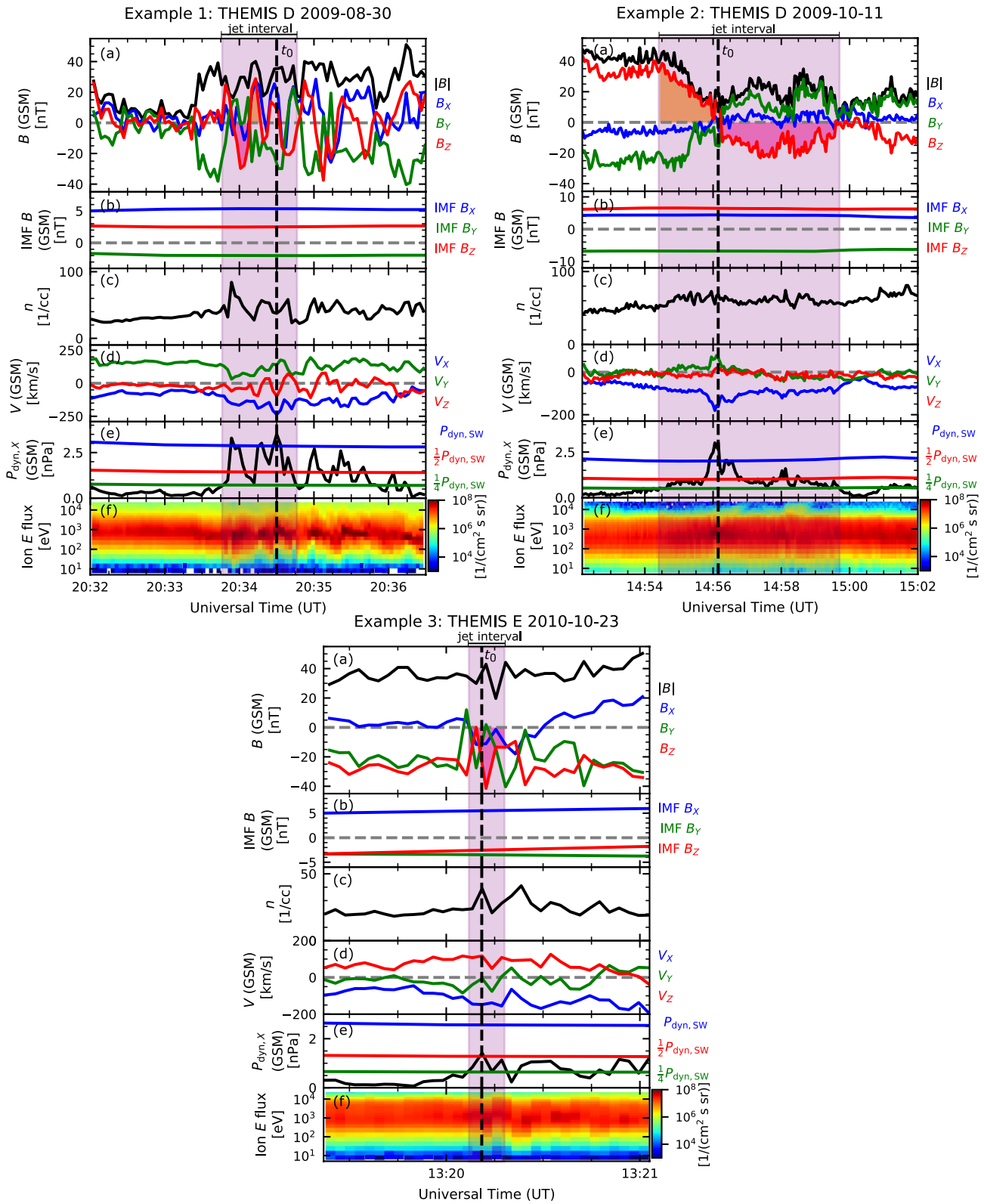
Example 1: THEMIS D 2009-08-30
Example 2: THEMIS D 2009-10-11
Example 3: THEMIS E 2010-10-23
jet interval
$t_0$
(a)
(b)
(c)
(d)
(e)
(f)
B (GSM) [nT]
IMF B (GSM) [nT]
n [1/cc]
V (GSM) [km/s]
$P_{dyn,X}$ (GSM) [nPa]
Ion E flux [eV]
|B|
$B_X$
$B_Y$
$B_Z$
IMF $B_X$
IMF $B_Y$
IMF $B_Z$
$V_X$
$V_Y$
$V_Z$
$P_{dyn,SW}$
$\frac{1}{2}P_{dyn,SW}$
$\frac{1}{4}P_{dyn,SW}$
[1/(cm$^2$ s sr)]
20:32
20:33
20:34
20:35
20:36
14:54
14:56
14:58
15:00
15:02
13:20
13:21
Universal Time (UT)

**Figure 1.**

**Table 1**
*Parameters of the Three Example Jet Events of Figure 1*

| | $F$ | $\alpha_Z$ | IMF $B_Z$ | Max $B_Z$ in jet | Min $B_Z$ in jet | Longest $B_Z > 0$ period in jet | Longest $B_Z < 0$ period in jet | $Q_\parallel$ or $Q_\perp$ |
|---|---|---|---|---|---|---|---|---|
| Example 1 | 0.46 | 25.1° | 2.50 nT | 28.7 nT | −29.7 nT | 9 s | 14 s | $Q_\parallel$ |
| Example 2 | 0.22 | 55.7° | 6.47 nT | 38.4 nT | −23.1 nT | 110 s | 202 s | $Q_\perp$ |
| Example 3 | −0.08 | 26.6° | −2.71 nT | −3.06 nT | −36.9 nT | 0 s | 12 s | $Q_\parallel$ |

*Note*. Relative radial position $F$ Between the Bow Shock ($F = 1$) and the magnetopause ($F = 0$), Interplanetary Magnetic Field (IMF) cone angle in the geocentric solar magnetospheric $X$-$Z$ plane $\alpha_Z$ (See Equation 2) and IMF $B_{Z,GSM}$ at $t_0$, the Maximum $B_{Z,GSM}$ in a jet, the minimum $B_{Z,GSM}$ in a jet, the duration of the longest southward period in a jet, the duration of the longest northward period in a jet, and the hemisphere (quasi-parallel or quasi-perpendicular; see the text for description) the jet was observed in.

$$F = (r - r_{MP})/(r_{BS} - r_{MP}). \quad (1)$$

Here, $r$ is the radial distance of the spacecraft from the Earth, and the distance of the bow shock $r_{BS}$ and the distance of the magnetopause $r_{MP}$ are measured along that same line. Due to uncertainties of the models, part of the observations did not fit between the expected bow shock and magnetopause locations. For instance, the jet in Example 3 in Figure 1 was observed at $F = -0.08$ (Table 1), that is, outside the model magnetosheath, even though the spacecraft was in the magnetosheath. In this study, we exclude observations outside the model magnetosheath values $F \in [-0.1,1.1]$. 3% of jet interval observations and 5% of non-jet magnetosheath observations did not fit in this range.

Suvorova et al. (2010) have reported that the location of the subsolar magnetopause may be inflated by up to 30% during quasi-radial IMF conditions. According to Suvorova and Dmitriev (2015, 2016), these expansions may be missed when using the Shue et al. (1998) magnetopause model and OMNI solar wind data. In this statistical study, we have chosen the representative magnetopause bin as $F \in [-0.1,0.3)$ to allow for such uncertainties in the models. Furthermore, in Figure S3 we show that the conclusions of this study are not sensitive to small changes in $F$. The OMNI data set consists of solar wind and IMF measurements that have been made at the L1 point and propagated to the Earth's bow shock (King & Papitashvili, 2005). Naturally, there is uncertainty in the data due to the applied time-shift and due to the evolution of the structures in the solar wind. Nevertheless, as we use 5-min averages, we are confident that the data are reliable for our purposes of obtaining the general IMF conditions.

After jets and non-jet observations have been classified by their relative radial positions between the magnetopause and the bow shock, we study the $B_Z$ observations. Principally, we look at the $B_Z$ distributions separately during northward (defined here as $B^{IMF}_{Z,GSM} > 0$) and southward IMF ($B^{IMF}_{Z,GSM} < 0$). In previous studies of the subsolar magnetosheath (e.g., Archer & Horbury, 2013; Plaschke et al., 2013; Vuorinen et al., 2019), jet occurrence has been observed to be strongly controlled by the IMF cone angle: jets mostly occur during low IMF cone angle conditions. Note that in the subsolar region, where the shock normal is approximately aligned with the Earth-Sun line, the IMF cone angle is in good agreement with shock obliquity angle $\theta_{Bn}$. We know that the upstream IMF conditions affect the magnetosheath field topology and, thus, we can

**Figure 1.** Time series of Time History of Events and Macroscale Interactions during Substorms observations for three different magnetosheath intervals with jets. The panels include: (a) magnetic field in Geocentric Solar Magnetospheric (GSM) coordinates, (b) OMNI interplanetary magnetic field data in GSM coordinates, (c) number density, (d) velocity in GSM coordinates, (e) earthward dynamic pressure (black) and OMNI solar wind dynamic pressure (1x: blue, 1/2x: red, 1/4x: green), and (f) ion energy flux density. The jet intervals are highlighted in purple shading and the longest periods of northward and southward $B_Z$ within the jet intervals are highlighted in orange and magenta, respectively. $t_0$ denotes the moment of highest ratio between the magnetosheath and the solar wind dynamic pressures within the jet.

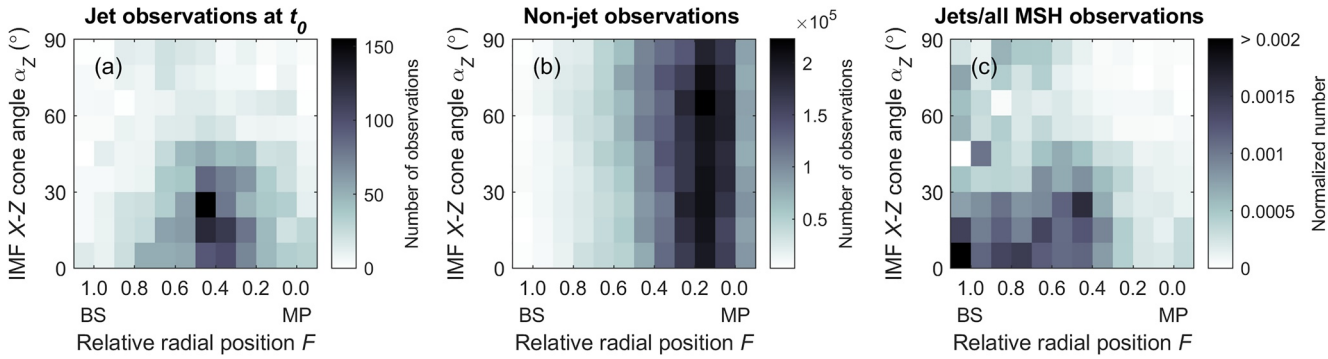


**Figure 2.** Maps showing the numbers of (a) jet observations taken at the moment $t_0$ of highest ratio of the earthward dynamic pressure and the solar wind dynamic pressure and (b) all non-jet observations as functions of the relative radial position $F$ between the bow shock ($F = 1$) and the magnetopause ($F = 0$) and the interplanetary magnetic field cone angle $\alpha_Z$ in the geocentric solar magnetospheric $X$-$Z$ plane. Map (c) shows the distribution of jet observations (at $t_0$) normalized by the distribution of all magnetosheath (MSH) observations.

expect this cone angle dependency to affect the $B_Z$ distribution of jets in comparison to all the non-jet magnetosheath observations in our data set. We consider these factors by sampling the non-jet magnetosheath such that the samples follow the same IMF cone angle distribution as the jet occurrence at a given relative position in the magnetosheath. Because we are studying $B_Z$, we use the IMF cone angle in the $X$-$Z$ plane for consistency:

$$\alpha_Z = \arctan\left|B_Z^{\mathrm{IMF}}/B_X^{\mathrm{IMF}}\right| \in [0°, 90°). \tag{2}$$

It is also important to check whether there is a hemispheric bias that affects the comparison of $B_Z$ observations within jets to those in non-jet intervals. We test this by separating the $X$-$Z$ plane into quasi-parallel and quasi-perpendicular hemispheres based on the $Z$ hemisphere that $\alpha_Z$ opens toward. Note that we do not consider where the quasi-parallel region is located exactly. We are only interested in whether more of it is expected on the positive or negative $Z$ hemisphere of the magnetosheath.

Figure 2 shows how the jet observations (at $t_0$; Figure 2a) and the non-jet observations (Figure 2b) are distributed in the 2D $F$-$\alpha_Z$ parameter space. These distributions are affected by non-uniform sampling due to the spacecraft orbits, so Figure 2c shows the jet occurrence normalized by all magnetosheath observations. The figures illustrate the need for sampling: there is a clear difference between the jet and non-jet distributions in both dimensions. The samples of non-jet intervals are generated with the popular method of inverse transform sampling (e.g., Ross, 2013) applying pseudorandom numbers from a Mersenne Twister generator (Matsumoto & Nishimura, 1998). We generate samples of non-jet intervals that follow the relative radial position $F$ and IMF cone angle $\alpha_Z$ distributions of the jets. The lengths of the non-jet intervals are also sampled from the lengths of jet intervals. The sampling algorithm is explained in detail in Text S1, where we have also included an illustration (Figure S1).

We are also interested in the variability of $B_Z$ within the jet intervals and how that compares to the variability in non-jet intervals. When studying this, we compare the $B_Z$ minima and maxima of jet intervals with those of non-jet intervals. As examples, Table 1 presents the minima and maxima of the example jet intervals in Figure 1. The table also includes the longest northward and southward $B_Z$ periods within the jets, and these are highlighted in orange and magenta, respectively, in the figure. Similarly, we compare the durations of these periods within jets to those within non-jet intervals.

We note that when comparing all observations (data points) in the intervals, the long-duration intervals are over-represented. On the other hand, when comparing interval minima and maxima, short-duration intervals are over-represented. Naturally, the whole length of the interval also introduces an upper limit for the durations of the longest southward or northward periods within the interval. As the lengths of non-jet intervals are sampled from the distribution of jet interval lengths to study jet and non-jet intervals of similar durations, this also applies for non-jet intervals. Therefore, the durations presented here for the southward and northward periods in non-jet intervals do not necessarily represent the actual lengths of these periods

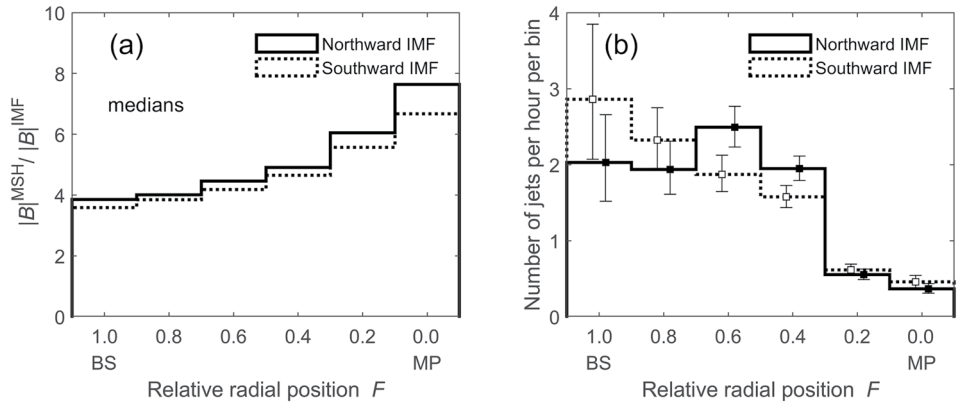


**Figure 3.** (a) The medians of the magnetosheath magnetic field magnitude normalized by the upstream interplanetary magnetic field (IMF) field magnitude as functions of the relative radial position during northward (solid line) and southward IMF (dotted line). (b) The number of jets observed by the spacecraft per hour within different bins of relative radial positions in the magnetosheath during northward (solid line) and southward IMF (dotted line). The error bars represent 95% binomial proportion confidence intervals obtained with the Clopper-Pearson method.

in the magnetosheath, as the periods may continue outside of the interval limits of the chosen interval. However, this also applies to jets, and we argue that it is important to compare the $B_Z$ observations in jet intervals to $B_Z$ observations in similar-duration non-jet intervals.

We estimate sampling error and uncertainty by comparing multiple samples of non-jet intervals. We generate 500 non-jet samples each consisting of the same number of intervals as the corresponding jet sample. Then we compare the $B_Z$ distributions of these different samples to each other by studying their statistics (e.g., medians). Once we have this sampling distribution for a particular statistic (e.g., medians of each of the 500 samples), we calculate its mean and also its 95% confidence interval defined by the 2.5th and 97.5th percentiles among the samples. In addition, we test the uncertainty of the jet interval distributions due to the finite number of jet intervals by applying non-parametric bootstrapping methods (e.g., Efron & Tibshirani, 1993). A bootstrap sample is generated by taking the set of jet intervals and randomly re-selecting the intervals with replacement. We form 500 such jet interval bootstrap samples and calculate the statistic for each of these samples. Again, we calculate the mean for this statistic and its 95% confidence interval. The conclusions of this study are not sensitive to bootstrapping, as they do not change when only using raw jet data. An example of this is provided in Figure S2.

When presenting numerical results, we always present these sample-averaged means and the 95% confidence intervals. However, in the histogram plots of Section 3.2, we only plot the observed jet sample and one random non-jet sample. The plotted non-jet sample is 20 times the size of the jet sample to decrease sampling error. Any deviations from these practices are mentioned separately.

## 3. Results

### 3.1. $B_Z$ Distributions Throughout the Magnetosheath

As we are particularly interested in the effect jets may have on reconnection during northward IMF, it is important to study whether jets can propagate to the magnetopause under such conditions when the magnetic pile-up layer forms in front of the magnetopause. Figure 3a shows the ratio of magnetosheath $|B|$ to solar wind $|B|$ at different radial positions $F$ in the magnetosheath for both northward (solid line) and southward (dotted line) IMF. We can see the effect of magnetic pile-up during northward IMF: the magnetic field magnitude close to the magnetopause is larger than during southward IMF. In Figure 3b, we present the number of jets the spacecraft observed per hour per bin as a function of $F$ both during northward and southward IMF. We can see that the number of observed jets per hour does not differ for northward and southward IMF close to the magnetopause. Therefore, the magnetic pile-up layer does not seem to affect the likelihood of jets reaching the magnetopause.

In Figures 4a and 4b, we present the distributions of $B_Z$ observations in jet intervals and non-jet magnetosheath samples as functions of $F$ during northward (Figure 4a) and southward IMF (Figure 4b). Both during northward and southward IMF, we can see that all the distributions broaden toward the magnetopause due to field line draping, but the effect is stronger during northward IMF. The jet and non-jet distributions are generally very similar throughout the magnetosheath both during northward and southward IMF. However, during northward IMF, the distributions of jet and non-jet interval observations are different close to the magnetopause: the non-jet magnetosheath exhibits much stronger northward values of $B_Z$ here. Studying the right-most bin $F \in [-0.1,0.1)$ further, we find that observing $B_Z$ opposite to the IMF $B_Z$ is generally as likely in jets as in non-jet intervals. During northward IMF, the likelihoods of observing southward $B_Z$ are: $36^{+9}_{-9}$% (mean and the 95% confidence interval) for jet interval observations and $24^{+11}_{-10}$% for the non-jet sample observations. The fractions of northward $B_Z$ during southward IMF are $18^{+6}_{-6}$% for jet interval observations and $27^{+11}_{-10}$% for non-jet observations. In Figure S2, we present the same figure using only raw jet data, not data averaged from bootstrap samples. The conclusions remain unchanged when using raw jet data.

We also look at the extreme values of $B_Z$ within jet and non-jet intervals. This helps us determine whether the variability introduced by jets is of the same order as the inherent variability of the magnetosheath. We do this by investigating the distributions of interval maxima and minima. We have plotted the interval maxima (minima) during northward IMF in Figure 4c (Figure 4e) and during southward IMF in Figure 4d (Figure 4f). It is generally more common for a jet interval than for a non-jet interval to exhibit $B_Z$ of opposite polarity to the IMF $B_Z$ at some point within the interval. These values of opposite $B_Z$ also tend to be stronger in magnitude within jets. Figure 4e shows that the distributions of interval minima during northward IMF are very different between jets and non-jet intervals. A significantly larger fraction of jets than non-jet intervals exhibit southward fields close to the magnetopause ($F \in [-0.1,0.1)$): $73^{+8}_{-11}$% and $34^{+10}_{-9}$%, respectively.

### 3.2. $B_Z$ Distributions Close to the Magnetopause

Next, we take a closer look at the $B_Z$ observations near the magnetopause. We choose the interval $F \in [-0.1,0.3)$ due to a larger sample size than the interval $F \in [-0.1,0.1)$ that we were looking at before. The results are not very different between these two intervals (see Figure S3 for details on the sensitivity of $F$ interval selection). In Figures 5a and 5b, we present the $B_Z$ distributions separately for northward and southward IMF. Southward $B_Z$ is typically only slightly more common in jets than in non-jet intervals during northward IMF, and the non-jet magnetosheath typically exhibits slightly larger $B_Z$. However, northward $B_Z$ is approximately as common within jets as within non-jet intervals during southward IMF. We can see in Figure 5a that during northward IMF, the jet and non-jet distributions peak at similar values. The medians are $4.4^{+1.4}_{-1.8}$nT for jet and $8.6^{+2.4}_{-2.2}$nT for non-jet observations. $37^{+6}_{-5}$% of jet interval observations and $26^{+6}_{-5}$% of non-jet interval observations are southward. Figure 5b shows that, during southward IMF, the differences between the jet interval observations and the non-jet observations are noticeably smaller. The medians are $-9.0^{+1.5}_{-1.4}$nT for jet and $-9.3^{+1.7}_{-1.9}$nT for non-jet observations. $25^{+4}_{-4}$% of jet observations and $23^{+5}_{-5}$% of non-jet observations are northward.

In Figures 5c and 5d, we present the interval minima during northward IMF and maxima during southward IMF, thus focusing on $B_Z$ of the opposite polarity to the IMF $B_Z$. We can clearly see that it is much more common for a jet to exhibit an extremum of opposite polarity to the IMF $B_Z$ than for a non-jet interval. During northward IMF (Figure 5c), $72^{+5}_{-6}$% of jets have a southward minimum within them in comparison to $40^{+5}_{-6}$% of non-jet intervals. This means that a significantly larger proportion of non-jet intervals do not contain any opposite $B_Z$. The medians are $-7.3^{+1.4}_{-1.3}$nT for jets and $3.3^{+1.7}_{-1.6}$nT for non-jet intervals. During southward IMF (Figure 5d), $62^{+6}_{-5}$% of jets and $37^{+6}_{-4}$% of non-jet intervals have a northward maximum within them. The medians are $5.2^{+1.6}_{-2.3}$nT for jets and $-3.6^{+1.4}_{-1.4}$nT for non-jet intervals.

We also calculated the percentages of southward $B_Z$ within those jet and non-jet intervals that did contain some southward $B_Z$ during northward IMF and vice versa (not shown). We find that the magnetic field within jets is more variable than in non-jet intervals in the sense that if a non-jet interval contains $B_Z$ opposite to the IMF $B_Z$, that polarity is maintained in a larger portion of the interval than in the case

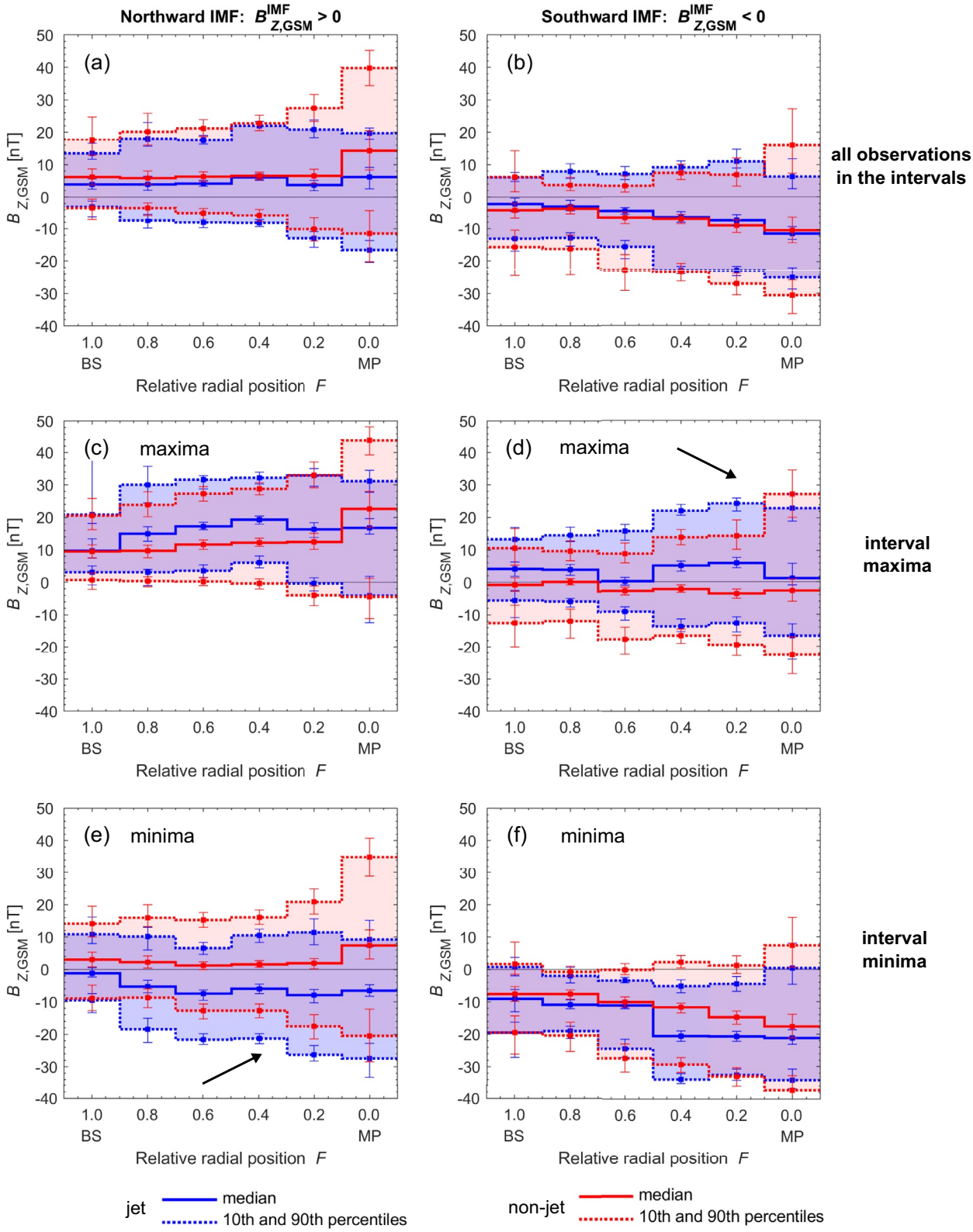
Northward IMF: $B^{IMF}_{Z,GSM} > 0$
Southward IMF: $B^{IMF}_{Z,GSM} < 0$
(a)
(b)
(c) maxima
(d) maxima
(e) minima
(f) minima
$B_{Z,GSM}$ [nT]
Relative radial position $F$
BS
MP
all observations in the intervals
interval maxima
interval minima
jet
non-jet
median
10th and 90th percentiles

**Figure 4.**

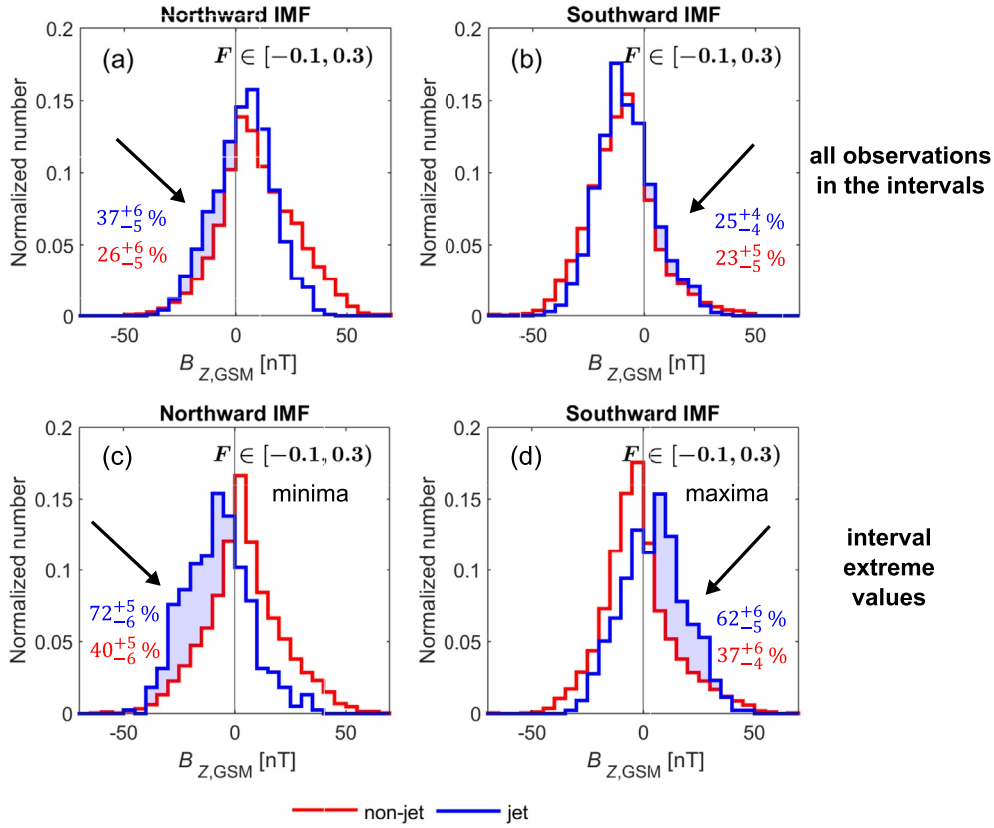


**Figure 5.** Distributions of $B_{Z,GSM}$ in jet (blue) and non-jet intervals (red) at $F \in [-0.1, 0.3)$ close to the magnetopause during (a, c) northward interplanetary magnetic field (IMF) and (b, d) southward IMF. Plots (a, b) show all interval observations and plots (c, d) show the interval minima for northward IMF and maxima for southward IMF. The arrows point at the sections that are interesting for reconnection—that is, that of the opposite polarity to the prevailing IMF $B_Z$, and the percentages tell the fractions of these southward (northward) values during northward (southward) IMF.

of jet intervals. During northward IMF, those jet intervals typically have southward $B_Z$ for $48^{+9}_{-9}$% of their duration. For non-jet intervals this proportion is $80^{+14}_{-16}$%. Similarly, during southward IMF, northward $B_Z$ typically makes up $37^{+6}_{-6}$% of the duration of these jet intervals and $69^{+16}_{-15}$% of non-jet intervals.

### 3.2.1. Durations of Northward and Southward Periods Within Intervals

Next, we look into the jet and non-jet intervals and study how long the periods of southward $B_Z$ are during northward IMF and vice versa. In Figure 6, we present the durations of the longest southward periods during northward IMF (Figures 6a and 6c) and northward periods during southward IMF (Figures 6b and 6d) within the intervals. In Figures 6a and 6b, we can see that although it is more common for a jet interval than for a non-jet interval to contain some $B_Z$ of opposite polarity to the IMF $B_Z$, the durations of such periods are statistically shorter both during northward and southward IMF. During northward IMF, the median durations of southward $B_Z$ periods are $11^{+3}_{-1}$s for jets and $19^{+5}_{-3}$s for non-jet intervals. Including the intervals that did not contain any southward $B_Z$ (i.e., the longest period is 0 s), the medians are $6^{+2}_{-1}$s and $0^{+0}_{-0}$s, respectively.

**Figure 4.** The 10th, 50th (medians), and 90th percentiles of $B_{Z,GSM}$ of jet (blue) and non-jet interval (red) observations as functions of relative radial position $F$ between the magnetopause and the bow shock during (a, c, e) northward interplanetary magnetic field (IMF) and (b, d, f) southward IMF. Plots (a–b) show all interval observations, (c–d) interval maxima, and (e–f) interval minima. The percentiles have been averaged from 500 samples and the error bars represent their 95% confidence intervals. The arrows point at the sections that are interesting for reconnection—that is, $B_Z$ opposite polarity to the prevailing IMF $B_Z$ near the magnetopause.

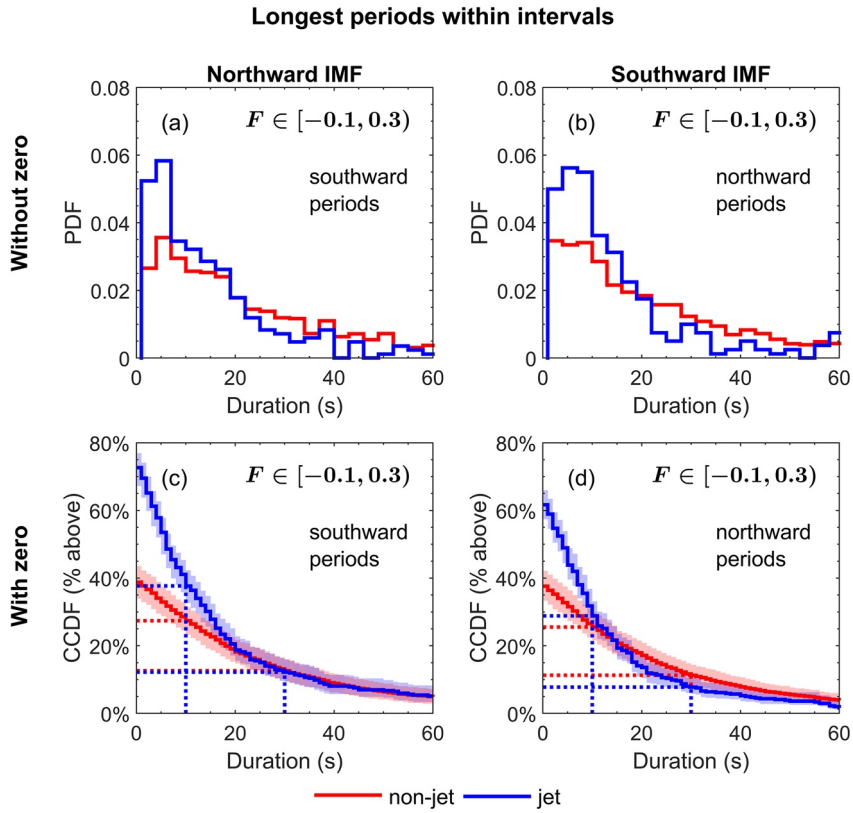


**Figure 6.** The durations of the longest periods of (a, c) southward $B_Z$ during northward interplanetary magnetic field (IMF) and (b, d) northward $B_Z$ during southward IMF within jet (blue) and non-jet (red) intervals. The distributions are presented as (a, b) probability density functions (PDFs) without durations of 0 s and as (c, d) complementary cumulative distribution functions (CCDFs, i.e., the percentages of observations above a certain duration) that also contain the 0 s durations. The CCDFs are the means of 500 samples and the highlighted regions are the 95% confidence intervals. Durations of 10 and 30 s are also separately marked.

During southward IMF, the medians of the lengths of northward periods are $10^{+1}_{-1}$s for jets and $18^{+4}_{-3}$s for non-jet intervals. Again, including the intervals with no northward $B_Z$, the medians are $4^{+1}_{-1}$s and $0^{+0}_{-0}$s.

Figures 6c and 6d display the complementary cumulative distribution functions (CCDFs), which show the percentages of observations above a certain duration. We have separately marked durations of 10 and 30 s. Table 2 presents the fractions of 0 s, ≥10s, and ≥30 s periods for northward and southward IMF. Short periods of opposite $B_Z$ are more common in jets than in non-jet intervals, but the prevalence of these periods in jets decreases rapidly with increasing duration. $41^{+5}_{-5}$% of jets during northward IMF contain southward periods of longer than 10 s in comparison to $29^{+4}_{-5}$% of non-jet intervals. Long periods of ≥30s seem to be as common in jet and non-jet intervals. During southward IMF, $32^{+5}_{-5}$% of jets have ≥10s northward periods within them, similar to $27^{+5}_{-5}$% of non-jet intervals. Looking at Figure 6c, we find that during northward IMF, southward periods up to 22 s (12 s as a conservative lower estimate) are more common within jets. Similarly, during southward IMF Figure 6d, northward periods up to 14 s (7 s as a conservative estimate) are more common within jets.

To study the strength of these opposite $B_Z$ pulses in jets, we investigate the $B_Z$ extremum values within the longest non-zero periods of opposite $B_Z$. During northward IMF, the minima are typically (median) $-10.9^{+1.3}_{-1.9}$nT. Similarly, during southward IMF, the maxima are typically $10.4^{+1.1}_{-1.4}$nT. These values are very similar for the periods in non-jet intervals: $-9.4^{+2.1}_{-2.3}$nT during northward IMF and $9.3^{+3.0}_{-2.3}$nT during southward IMF.

**Table 2**
*The Durations of the Longest Southward Periods During Northward Interplanetary Magnetic Field (IMF) and Northward Periods During Southward IMF Within Jets and Non-Jet Intervals Near the Magnetopause*

| | Northward IMF: $B_Z < 0$ periods | | Southward IMF: $B_Z > 0$ periods | |
|---|---|---|---|---|
| Duration | Jets | Non-jet intervals | Jets | Non-jet intervals |
| 0 s | $28^{+5}_{-5}\%$ | $61^{+6}_{-5}\%$ | $38^{+5}_{-5}\%$ | $62^{+5}_{-5}\%$ |
| ≥ 10s | $41^{+5}_{-5}\%$ | $29^{+4}_{-5}\%$ | $32^{+5}_{-5}\%$ | $27^{+5}_{-5}\%$ |
| ≥ 30s | $13^{+4}_{-4}\%$ | $13^{+4}_{-3}\%$ | $8^{+3}_{-3}\%$ | $12^{+3}_{-4}\%$ |

*Note*. The results are presented as percentages of periods of 0 s, ≥ 10 s, and ≥ 30 s.

Nykyri et al. (2019) reported an event that occurred on December 25, 2015, in which a substorm onset was observed during northward IMF. Strong pulses of southward $B_Z$, associated with dynamic pressure enhancements, had been observed earlier in the magnetosheath by the Magnetospheric Multiscale spacecraft (MMS). According to their multipoint measurements and timing analysis, the chain of events leading to the substorm onset at ~08:17 UT could have started by magnetopause reconnection triggered by the southward pulses associated with jets observed by MMS at around 08:00:20 UT. We use MMS1 FGM data (Russell et al., 2016) to determine the durations and $B_Z$ minima of the southward pulses observed by Nykyri et al. (2019). At around 08:00:19 UT, MMS1 observed a strong pulse of $B_Z = -24$nT and 4 s in duration. Other strong pulses also highlighted by Nykyri et al. (2019) were observed at 08:06:54 UT, 08:07:14 UT, 08:09:44 UT, and 08:10:16 UT. In Figure 7, we compare these pulses (black dots) to our results of southward periods in jet (blue dots) and non-jet intervals (red dots) during northward IMF. In Figure 7a, we use the interval minima and the durations of the southward periods around the minima. In Figure 7b, we use the longest southward periods within the intervals and the minima of these particular periods. The samples used for plotting are the observed jet sample and a non-jet sample of the same size. We have drawn a rectangle (solid line) that contains all the data points of equal or stronger southward $B_Z$ and equal or longer durations than the $B_Z = -24$nT and 4 s pulse observed at 08:00:19 UT (shown as a larger black dot). In Figure 7a, we find that these types of pulses were observed in $13^{+4}_{-4}\%$ of jets and $5^{+3}_{-3}\%$ of non-jet intervals. In Figure 7b, on the other hand, the rectangle contains $12^{+4}_{-4}\%$ of jets and $6^{+2}_{-3}\%$ of non-jet intervals. Thus, while strong southward pulses similar to the one observed by Nykyri et al. (2019) are slightly more common within jets than in non-jet magnetosheath, such pulses are not frequently observed.

### 3.2.2. Effect of Quasi-Parallel and Quasi-Perpendicular Hemispheres of the Magnetosheath

In Figure 8, we present the $B_Z$ distributions on the quasi-perpendicular and quasi-parallel hemispheres separately, to check if hemispheric differences could explain the effects seen earlier. Figures 8a–8d show the $B_Z$ distributions of all measurements during the intervals, and Figures 8e–8h show the interval minima during northward IMF and maxima during southward IMF. The percentages of $B_Z$ observations of opposite polarity to the IMF $B_Z$ are presented in the plots. The general conclusions of the previous sections hold for both hemispheres: distributions of all $B_Z$ measurements made during the intervals are similar for jet and non-jet intervals, but it is more likely for a jet interval than for a non-jet interval to exhibit an extremum $B_Z$ opposite to the IMF $B_Z$. The differences between the quasi-parallel and quasi-perpendicular hemispheres are small and within uncertainty.

### 3.2.3. Cone Angle Dependency

So far, we have compared the distribution of $B_Z$ measurements taken within jets to those taken within non-jet magnetosheath intervals during similar IMF cone angle $\alpha_Z$ conditions. Lastly, in Figure 9, we investigate the sensitivity of our results to this IMF obliquity by plotting the distributions of all jet interval

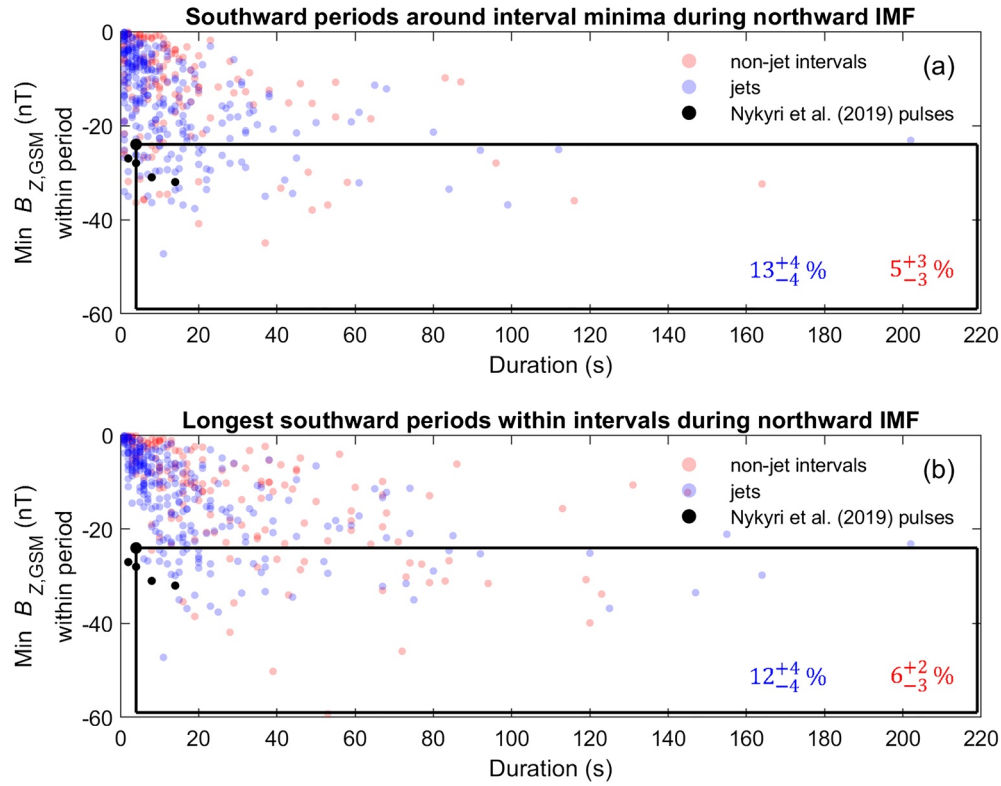


**Figure 7.** Southward periods within jet (blue) and non-jet (red) intervals during northward interplanetary magnetic field (IMF). The strong southward pulses reported by Nykyri et al. (2019) (black) are shown for comparison. (a) $B_Z$ minima of intervals and the durations of the southward periods around these minima. (b) The longest southward periods within intervals and the $B_Z$ minima of these periods. The solid rectangle contains the periods that are stronger or equal or longer or equal in duration to the Nykyri et al. (2019) pulse of 4 s and $B_Z = -24$nT (larger black dot) that can be linked to the substorm onset via their timing analysis. The percentages represent the means and 95% confidence intervals obtained from 500 samples.

observations and non-jet observations as functions of $\alpha_Z$, using their 10th, 50th, and 90th percentiles. As reported in earlier studies (e.g., Plaschke et al., 2013), jets are mostly observed during low IMF cone angles. In fact, around 80% of jets in our data set were observed for $\alpha_Z < 45°$. Therefore, the results on the differences between jets and non-jet magnetosheath presented in previous subsections primarily relate to the two leftmost bins in Figures 9a and 9b. However, we find that these differences between jet and non-jet percentiles only increase with an increasing cone angle, as the non-jet percentiles move higher (lower) for northward (southward) IMF while the jet distributions remain largely the same. This indicates that such differences exist for all cone angles. To further investigate this, we divide the data into two subsets: low cone angles $\alpha_Z \in [0°,45°)$ and high cone angles $\alpha_Z \in [45°,90°]$, and find that the results presented for the whole data set match well with the results of the low cone angle subset. During high cone angles, the differences between the jet and non-jet $B_Z$ distributions tend to be larger still. These results are presented in the Table S1.

## 4. Discussion

We have studied the magnetic field component $B_{Z,GSM}$ within magnetosheath jets and similar-duration non-jet magnetosheath intervals to determine whether the magnetic field within jets can be expected to have the potential to affect local magnetic reconnection at the subsolar magnetopause, bounded by a 30° cone

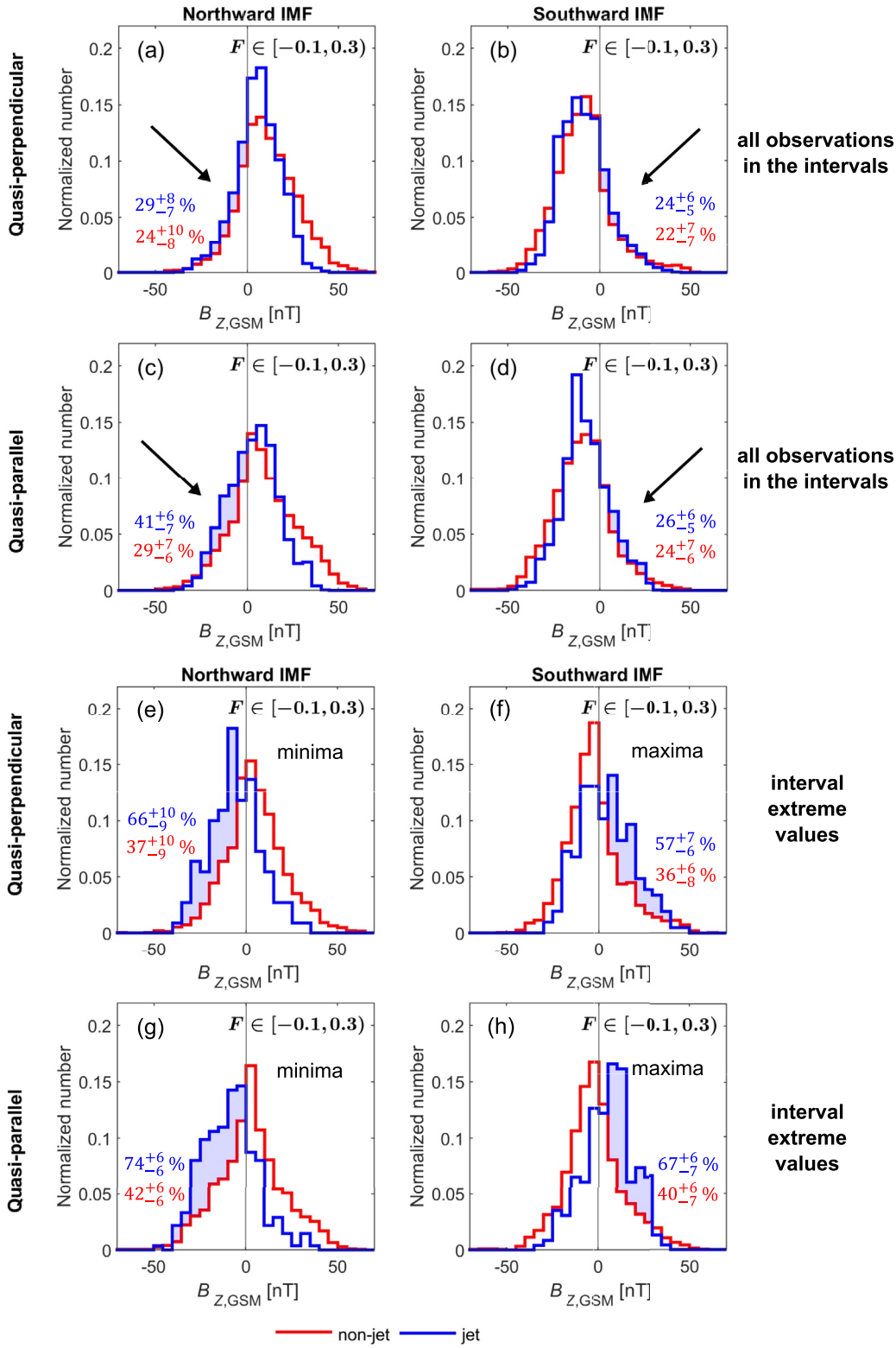


**Figure 8.** Distributions of jet (blue) and non-jet (red) interval $B_{Z,GSM}$ observations on the quasi-perpendicular and quasi-parallel hemispheres of the $X$-$Z$ plane at the $F \in [-0.1, 0.3)$ region close to the magnetopause during (a, c, e, g) northward interplanetary magnetic field (IMF) and (b, d, f, h) southward IMF. Plots (a–d) show all interval observations and plots (e–h) show interval minima during northward IMF and maxima during southward IMF. The arrows point at the sections that are interesting for reconnection—that is, that of the opposite polarity to the IMF $B_Z$, and the percentages tell the fractions of these southward (northward) values during northward (southward) IMF.

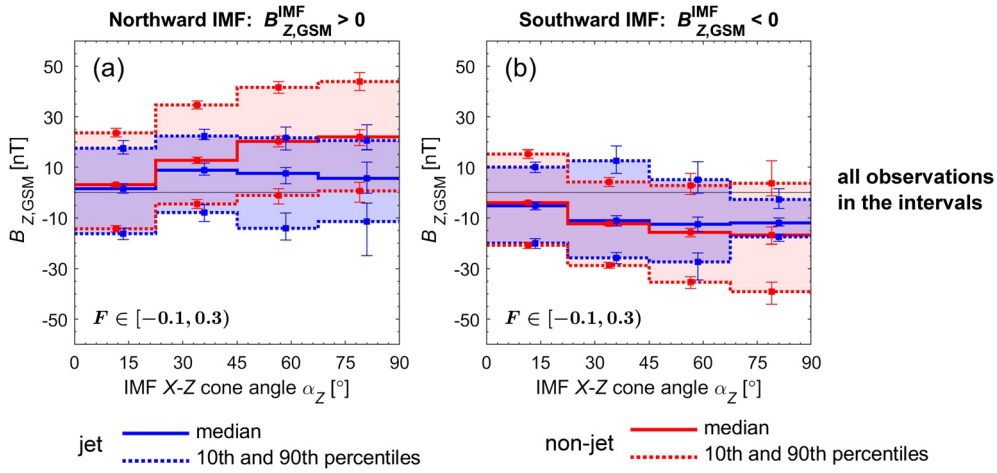


**Figure 9.** The 10th, 50th (medians), and 90th percentiles of $B_{Z,GSM}$ of all jet interval observations (blue) and similar non-jet magnetosheath samples (red) during (a) northward interplanetary magnetic field (IMF) and (b) southward IMF as functions of the IMF cone angle in the $X$-$Z$ plane, $\alpha_Z$. The data are from the region $F \in [-0.1, 0.3)$. The percentiles have been averaged from 500 samples and the error bars represent their 95% confidence intervals. The non-jet samples are 10 times larger to reduce uncertainty.

around the Sun-Earth line (determined by the extent of the Plaschke et al., 2013 data set). The situation may be different in higher latitudes. According to our results, jets are observed close to the magnetopause as frequently during northward and southward IMF: on average a spacecraft close to the magnetopause observes one jet in two hours. This indicates that the presence of a magnetic pile-up layer during northward IMF does not affect the penetration of jets toward the magnetopause. Our results suggest that, within uncertainty, $B_Z$ of opposite polarity to the IMF $B_Z$ is typically approximately as common within jets as within non-jet intervals close to the magnetopause: $37^{+6}_{-5}$% of jet observations versus $26^{+6}_{-5}$% of non-jet observations during northward IMF and $25^{+4}_{-4}$% versus $23^{+5}_{-5}$%, respectively, during southward IMF. However, the key result is that when we consider the minimum and maximum values within individual intervals, it is significantly more likely for a jet interval than for a non-jet interval to contain southward $B_Z$ during northward IMF ($72^{+5}_{-6}$% of jet intervals vs. $40^{+5}_{-6}$% of non-jet intervals) or northward $B_Z$ during southward IMF ($62^{+6}_{-5}$% vs. $37^{+6}_{-4}$%, respectively). These numbers are representative of low IMF cone angle $\alpha_Z$ conditions, when jets are mostly observed, but the differences between jet and non-jet distributions become in fact higher during high cone angles. These results indicate that jets may have potential to locally affect the state of reconnection at the magnetopause via their magnetic fields.

We tested whether the results differ on the quasi-parallel and quasi-perpendicular $Z$ hemispheres and found that the results are the same within uncertainty, and the previous conclusions remain. Thus, our results are not explained by hemispheric differences. We have also tested whether the results depend on biases within the data set: dipole tilt due to seasonal changes and differences between $+Z$ and $-Z$ hemispheres due to orbital bias in our data set (not shown). We have found that these do not seem to explain our results or change the conclusions.

What causes this $B_Z$ difference is beyond the scope of this study, but possible factors that could affect the magnetic field inside jets could be related to the nature of the quasi-parallel shock, for example, passage of foreshock waves and turbulence into the magnetosheath within jets, or local effects such as field line draping around the jets. Previous studies have reported wave activity in and around jets (Gunell et al., 2014; Karlsson et al., 2018) and shown that there is a small (10°) effect of magnetosheath field becoming more aligned with the jet velocity (Plaschke, Jernej, et al., 2020). According to our results, $B_Z$ observations within jet intervals are not dependent on the IMF $\alpha_Z$ cone angle, while this parameter controls the non-jet magnetosheath $B_Z$ distribution. One would expect that if local field line draping around jets was the responsible phenomenon, the effect of IMF $\alpha_Z$ cone angle should also be seen in the $B_Z$ distribution of jet interval observations. In general, the effect of high-speed jets on the surrounding magnetosheath plasma and magnetic

field may be highly complex in three dimensions, which could possibly explain why the $B_Z$ distribution of jets is similar during varying IMF $\alpha_Z$ cone angle conditions, and why the field is more variable within a jet interval.

The lengths and strengths of southward and northward periods within jets are also important factors for assessing their potential effects on reconnection. The longest periods of $B_Z$ opposite to the IMF within jet intervals are typically $11^{+3}_{-1}$s during northward IMF and $10^{+1}_{-1}$s during southward IMF. Such periods in jets tend to be shorter in duration than the periods in non-jet intervals, as for non-jet intervals typical durations are $19^{+5}_{-3}$s during northward IMF and $18^{+4}_{-3}$s during southward IMF. The median strengths of these pulses are similar in jets and non-jet intervals: $-10.9^{+1.3}_{-1.9}$nT versus $-9.4^{+2.1}_{-2.3}$nT, respectively, during northward IMF and $10.4^{+1.1}_{-1.4}$nT versus $9.3^{+3.0}_{-2.3}$nT during southward IMF. Nevertheless, as these periods are indeed more common within jets, southward periods of up to ≥22s (12 s as a conservative lower estimate) are more common within jets than in non-jet intervals during northward IMF. During southward IMF, northward periods of up to 14 s (7 s as a conservative lower estimate) are more common within jets than in non-jet intervals.

Finally, we note that it is not well understood what kind of magnetic field fluctuations are sufficient for locally triggering or suppressing magnetopause reconnection. We can assume that the strength of the pulse and its duration are both important parameters. Our results show that while such pulses of opposite polarity to the IMF $B_Z$ are more common within jets, their timescale tends to be short (from the more common periods of a few seconds to a few tens of seconds). The shorter the period, higher the occurrence in jets relative to the occurrence in non-jet intervals. Therefore, to determine the potential of jets to affect local magnetopause reconnection, we would need a better understanding on the timescales required for reconnection to occur. Furthermore, the link between southward magnetic field within a jet and jet-related local reconnection is not yet clear and should be further studied. As jets are localized structures and these periods of opposite $B_Z$ are short, their possible effects on magnetopause reconnection can be expected to be localized in both time and space. However, as in the event observed by Nykyri et al. (2019), localized reconnection events may at times have global magnetospheric consequences.

A few studies have discussed foreshock/jet related magnetopause reconnection. Zhang et al. (1997) considered the propagation of foreshock magnetic fluctuations into the magnetosheath and suggested that these fluctuations could cause periods of southward $B_Z$ during northward IMF and possibly trigger reconnection. They investigated the position of the magnetopause during low and high IMF cone angle conditions and found, within the accuracy of their data, no evidence of increased magnetopause erosion during low IMF cone angle conditions. Thus, they concluded that these fluctuations do not cause reconnection and argued that the timescale of the fluctuations is probably too short for reconnection. However, Kullen et al. (2019) studied the occurrence of two different types of flux transfer events (FTEs): FTE cascades with separation times <70 min and isolated FTEs with separation times ≥70 min. They found that while only 2–5% of FTE cascades in their data set occurred during low IMF cone angle (<30°) conditions, 16% of isolated FTEs occurred during these conditions. They suggested a link between magnetosheath jets and this subset of isolated FTEs as jet-related reconnection events could presumably produce isolated FTEs and explain the random spatial distribution of these FTEs. Karimabadi et al. (2014) have also previously reported a jet triggering a FTE (or a magnetic island) in their 2D hybrid simulations. As Plaschke et al. (2013) reported, jets can often be observed with relatively short recurrence times (median: 140 s). Multi-point reconnection caused by recurring jets could lead to formation of FTEs.

Observations by Hietala et al. (2018) and Nykyri et al. (2019) provide evidence for jet-induced reconnection. The kinds of the strong, negative $B_Z$ pulse observed by Nykyri et al. (2019) during northward IMF are estimated to occur in $13^{+4}_{-4}$% of jets in comparison to $6^{+2}_{-3}$% of non-jet intervals. Note that Nykyri et al. (2019) observed this pulse close to the bow shock while we study intervals close to the magnetopause. Using jet impact rates estimated by Vuorinen et al. (2019) based on the model introduced by Plaschke et al. (2016), we can make a rough estimation of how many this type of jets hit the subsolar magnetopause per hour. We estimate this impact rate to be 7 (5–10) jets per hour for jets with diameters larger than $1R_E$ perpendicular to their flow direction during northward IMF low cone angle (<30°) conditions. The percentages mentioned before apply for all jets at $F \in [-0.1, 0.3)$, also the jets smaller than $1R_E$ in diameter. Thus, we can take this estimation as a rough lower limit.

Although $B_{Z,\mathrm{GSM}}$ can be regarded as the most important parameter for magnetic reconnection at the magnetopause, many other parameters also affect reconnection: for example, plasma beta shear, flow shear, and current sheet thickness. The effect of jets on these parameters should be studied in more detail. Previous studies have indicated that variations to the local plasma conditions at the magnetopause can affect reconnection rates. For example, Laitinen et al. (2010) suggested based on their two-event case study that plasma beta variations caused by mirror mode waves with periods of the order of a minute can either introduce fluctuations to steady reconnection or trigger bursty reconnection. Hoilijoki et al. (2017) provided further evidence for this based on their global 2D-3V hybrid-Vlasov simulations. Mirror modes are typically observed downstream of the quasi-perpendicular shock.

Case studies of the magnetic structure of jets should be conducted in the future to help us understand why there are statistical differences between the magnetic field orientations within jet intervals and within non-jet intervals of similar duration. During our research, we have encountered low-frequency wave-like variations within jets (see Figure 1). The connection between the upstream foreshock wavefield and the magnetic field structure in jets should be investigated. Similarly, local field-line draping around the fast-moving jets should also be studied in detail. Most importantly, case studies should be conducted to find more examples of jets triggering magnetopause reconnection. Such observations along with simulations would help us to understand what kind of conditions are actually required for reconnection to take place due to a jet impact, for example, how long or strong the southward period within a jet should be. The high dynamic pressure of jet. allows for thinning of the magnetopause, which can lead to reconnection as observed by Hietala et al. (2018). This is a unique feature of jets, which can be expected to increase the "effectiveness" of jets in terms of reconnection.

## 5. Conclusions and Summary

In this study, we studied the $B_{Z,\mathrm{GSM}}$ within jets and within similar-duration non-jet magnetosheath intervals. The main results of this study can be listed as:

1. The magnetic pile-up layer that forms during northward IMF does not seem to affect the penetration of jets toward the magnetopause, as jets are observed as frequently close to the magnetopause during northward IMF as during southward IMF. On average, a spacecraft observes one jet in 2 h close to the magnetopause.
2. Taking the whole time intervals, observations of $B_Z$ opposite to the prevailing IMF $B_Z$ are typically roughly as common in jets as in similar-duration non-jet intervals close to the magnetopause. Such measurements constitute $37^{+6}_{-5}$% of jet and $26^{+6}_{-5}$% of non-jet observations during northward IMF and $25^{+4}_{-4}$% and $23^{+5}_{-5}$% of observations, respectively, during southward IMF.
3. However, it is more common for a jet interval than for a non-jet interval to exhibit some $B_Z$ of opposite polarity to the IMF $B_Z$ near the magnetopause: $72^{+5}_{-6}$% of jets versus $40^{+5}_{-6}$% of non-jet intervals during northward IMF and $62^{+6}_{-5}$% versus $37^{+6}_{-4}$% of intervals, respectively, during southward IMF. This means that most jets contain a pulse of opposite $B_Z$, while the majority of non-jet intervals do not contain any opposite $B_Z$.
4. The durations of the longest southward periods during northward IMF and northward periods during southward IMF are shorter within jets than in non-jet intervals close to the magnetopause. During northward IMF, the median durations of non-zero southward periods were $11^{+3}_{-1}$s for jets and $19^{+5}_{-3}$s for non-jet intervals. During southward IMF, the median lengths of non-zero northward periods were $10^{+1}_{-1}$s and $18^{+4}_{-3}$ s, respectively.
5. However, southward periods of up to 22s (conservative lower estimate 12s) are more common in jets than in non-jet intervals during northward IMF. Likewise, northward periods of up to 14s (conservative lower estimate 7s) are more frequently observed in jets than in non-jet intervals during southward IMF.
6. These longest pulses of opposite $B_Z$ are typically as strong in jets as in non-jet intervals. The medians of the extremum values are: $-10.9^{+1.3}_{-1.9}$nT in jets versus $-9.4^{+2.1}_{-2.3}$nT in non-jet intervals during northward IMF and $10.4^{+1.1}_{-1.4}$nT versus $9.3^{+3.0}_{-2.3}$nT during southward IMF.
7. Strong southward $B_Z$ pulses similar or stronger than the 4 s and $B_Z = -24$nT pulse reported by Nykyri et al. (2019) during northward IMF are slightly more common in jets than in non-jet intervals, but they

are not frequently observed. Such periods were observed in $13^{+4}_{-4}$% of jets and in $6^{+2}_{-3}$% of non-jet intervals near the magnetopause. Still, as jet impacts are so frequent, we make a rough estimate for jets with diameters $>1R_E$: such pulses would impact the subsolar magnetopause 5–10 times per hour during low IMF cone angle conditions.

8. The general $B_Z$ distribution in the near-magnetopause magnetosheath is dependent on the IMF obliquity: during northward (southward) IMF, $B_Z$ values tend to become higher (lower) with increasing IMF obliquity. However, the distribution within jets does not seem to be significantly affected by the obliquity. While jets are less common during high IMF cone angle conditions, the differences between the distributions of jet and non-jet interval $B_Z$ observations become larger with increasing IMF obliquity.

The main conclusion of this study is that close to the magnetopause jets contain more short-duration pulses of $B_Z$ opposite to the prevailing IMF than the non-jet magnetosheath. During northward IMF, the likelihood of observing some southward $B_Z$ in jets is 1.5–2.3 times the likelihood in non-jet intervals. During southward IMF, the likelihood of observing some northward $B_Z$ is 1.3–2.1 times the likelihood in non-jet intervals. In fact most jets (∼60–70%) exhibit some $B_Z$ of opposite polarity to the IMF. Therefore, jets introduce southward $B_Z$ to the magnetopause during northward IMF and northward $B_Z$ during southward IMF. The magnetic field within jets may have potential to affect local reconnection at the magnetopause: trigger it during northward IMF and suppress it during southward IMF. However, these periods of opposite $B_Z$ within jets are short, as typically the longest periods within a jet are around 10 s. Their typical strengths are around ±10nT. Thus, the significance of these effects depends on the question of what kind of pulses of $B_Z$ opposite to the IMF (e.g., how long-lasting and how strong in $B_Z$) are able to locally trigger or turn off reconnection at the magnetopause. Future studies are needed to answer to this question.

## Data Availability Statement

THEMIS and OMNI data can be accessed via, for example, NASA's Coordinated Data Analysis Web (https://cdaweb.gsfc.nasa.gov/). The magnetosheath and jet data set used in this study can be found at: https://osf.io/gf732/ (Plaschke, Hietala, & Angelopoulos, 2020).

**Acknowledgments**
The work in the University of Turku has been conducted in the framework of Finnish Centre of Excellence in Research of Sustainable Space. The work in the University of Turku was supported by the Jenny and Antti Wihuri Foundation and the Turku Collegium of Science and Medicine. The work at Imperial College was supported by Royal Society awards URF\R1\180671 and RGF\EA\181090. LV acknowledges the financial support of the Academy of Finland (Project #309939). The work of HH was also supported by NASA grant NNX17AI45G. FP is supported by the Austrian Science Fund (FWF): P 33285-N. We acknowledge NASA contract NAS5-02099 and V. Angelopoulos for use of data from the THEMIS Mission.

## References

Angelopoulos, V. (2008). The THEMIS Mission. *Space Science Reviews*, *141*(1), 5–34. https://doi.org/10.1007/s11214-008-9336-1

Archer, M. O., Hietala, H., Hartinger, M. D., Plaschke, F., & Angelopoulos, V. (2019). Direct observations of a surface eigenmode of the dayside magnetopause. *Nature Communications*, *10*(1), 615. https://doi.org/10.1038/s41467-018-08134-5

Archer, M. O., & Horbury, T. S. (2013). Magnetosheath dynamic pressure enhancements: Occurrence and typical properties. *Annales Geophysicae*, *31*(2), 319–331. https://doi.org/10.5194/angeo-31-319-2013

Auster, H. U., Glassmeier, K. H., Magnes, W., Aydogar, O., Baumjohann, W., Constantinescu, D., et al. (2008). The THEMIS fluxgate magnetometer. *Space Science Reviews*, *141*(1–4), 235–264. https://doi.org/10.1007/s11214-008-9365-9

Burgess, D., & Scholer, M. (2015). *Collisionless shocks in space plasmas*. Cambridge University Press.

Cassak, P. A., & Fuselier, S. A. (2016). Reconnection at Earth's dayside magnetopause. In W. Gonzalez, & E. Parker (Eds.), *Magnetic reconnection* (1st ed., pp. 213–276). Springer International Publishing. https://doi.org/10.1007/978-3-319-26432-5

Efron, B., & Tibshirani, R. J. (1993). *An introduction to the bootstrap*. Chapman & Hall.

Fairfield, D. H. (1967). The ordered magnetic field of the magnetosheath. *Journal of Geophysical Research*, *72*(23), 5865–5877. https://doi.org/10.1029/JZ072i023p05865

Gunell, H., Stenberg Wieser, G., Mella, M., Maggiolo, R., Nilsson, H., Darrouzet, F., et al. (2014). Waves in high-speed plasmoids in the magnetosheath and at the magnetopause. *Annales Geophysicae*, *32*(8), 991–1009. https://doi.org/10.5194/angeo-32-991-2014

Hietala, H., Laitinen, T. V., Andréeová, K., Vainio, R., Vaivads, A., Palmroth, M., et al. (2009). Supermagnetosonic jets behind a collisionless quasiparallel shock. *Physical Review Letters*, *103*(24), 245001. https://doi.org/10.1103/PhysRevLett.103.245001

Hietala, H., Phan, T. D., Angelopoulos, V., Oieroset, M., Archer, M. O., Karlsson, T., & Plaschke, F. (2018). In situ observations of a magnetosheath high-speed jet triggering magnetopause reconnection. *Geophysical Research Letters*, *45*(4), 1732–1740. https://doi.org/10.1002/2017GL076525

Hoilijoki, S., Ganse, U., Pfau-Kempf, Y., Cassak, P. A., Walsh, B. M., Hietala, H., et al. (2017). Reconnection rates and X line motion at the magnetopause: Global 2D-3V hybrid-Vlasov simulation results. *Journal of Geophysical Research: Space Physics*, *122*(3), 2877–2888. https://doi.org/10.1002/2016JA023709

Karimabadi, H., Roytershteyn, V., Vu, H. X., Omelchenko, Y. A., Scudder, J., Daughton, W., et al. (2014). The link between shocks, turbulence, and magnetic reconnection in collisionless plasmas. *Physics of Plasmas*, *21*(6), 062308. https://doi.org/10.1063/1.4882875

Karlsson, T., Kullen, A., Liljeblad, E., Brenning, N., Nilsson, H., Gunell, H., & Hamrin, M. (2015). On the origin of magnetosheath plasmoids and their relation to magnetosheath jets. *Journal of Geophysical Research: Space Physics*, *120*, 7390–7403. https://doi.org/10.1002/2015JA021487

Karlsson, T., Plaschke, F., Hietala, H., Archer, M., Blanco-Cano, X., Kajdič, P., et al. (2018). Investigating the anatomy of magnetosheath jets—MMS observations. *Annales Geophysicae*, *36*(2), 655–677. https://doi.org/10.5194/angeo-36-655-2018

King, J. H., & Papitashvili, N. E. (2005). Solar wind spatial scales in and comparisons of hourly Wind and ACE plasma and magnetic field data. *Journal of Geophysical Research*, *110*(A2). https://doi.org/10.1029/2004JA010649

Kullen, A., Thor, S., & Karlsson, T. (2019). The difference between isolated flux transfer events and flux transfer event cascades. *Journal of Geophysical Research: Space Physics*, *124*(10), 7850–7871. https://doi.org/10.1029/2019JA026629

Laitinen, T. V., Khotyaintsev, Y. V., André, M., Vaivads, A., & Rème, H. (2010). Local influence of magnetosheath plasma beta fluctuations on magnetopause reconnection. *Annales Geophysicae*, *28*(5), 1053–1063. https://doi.org/10.5194/angeo-28-1053-2010

Lucek, E. A., Horbury, T. S., Dandouras, I., & Re, H. (2008). Cluster observations of the Earth's quasi-parallel bow shock. *Journal of Geophysical Research*, *113*, 1–11. https://doi.org/10.1029/2007JA012756

Matsumoto, M., & Nishimura, T. (1998). Mersenne twister: A 623-dimensionally equidistributed uniform pseudo-random number generator. *ACM Transactions on Modeling and Computer Simulation*, *8*(1), 3–30. https://doi.org/10.1145/272991.272995

McFadden, J. P., Carlson, C. W., Larson, D., Ludlam, M., Abiad, R., Elliott, B., et al. (2008). The THEMIS ESA plasma instrument and in-flight calibration. *Space Science Reviews*, *141*(1–4), 277–302. https://doi.org/10.1007/s11214-008-9440-2

Merka, J., Szabo, A., Slavin, J. A., & Peredo, M. (2005). Three-dimensional position and shape of the bow shock and their variation with upstream Mach numbers and interplanetary magnetic field orientation. *Journal of Geophysical Research*, *110*(A4), 1–13. https://doi.org/10.1029/2004JA010944

Nykyri, K., Bengtson, M., Angelopoulos, V., Nishimura, Y., & Wing, S. (2019). Can enhanced flux loading by high-speed jets lead to a substorm? Multipoint detection of the Christmas Day substorm onset at 08:17 UT, 2015. *Journal of Geophysical Research: Space Physics*, *124*(6), 4314–4340. https://doi.org/10.1029/2018JA026357

Omelchenko, Y. A., Chen, L.-J., & Ng, J. (2021). 3D space-time adaptive hybrid simulations of magnetosheath high-speed jets. *Journal of Geophysical Research: Space Physics*, *126*(7), e2020JA029035. https://doi.org/10.1029/2020JA029035

Papitashvili, N. E., & King, J. H. (2020). *OMNI 1-min data set [data set]*. NASA Space Physics Data Facility. https://doi.org/10.48322/45bb-8792

Phan, T. D., Paschmann, G., Baumjohann, W., Sckopke, N., & Lühr, H. (1994). The magnetosheath region adjacent to the dayside magnetopause: AMPTE/IRM observations. *Journal of Geophysical Research*, *99*(A1), 121–141. https://doi.org/10.1029/93JA02444

Plaschke, F., Hietala, H., & Angelopoulos, V. (2013). Anti-sunward high-speed jets in the subsolar magnetosheath. *Annales Geophysicae*, *31*(10), 1877–1889. https://doi.org/10.5194/angeo-31-1877-2013

Plaschke, F., Hietala, H., & Angelopoulos, V. (2020). *Anti-sunward high-speed jets in the subsolar magnetosheath: Data sets*. Retrieved from https://osf.io/gf732/

Plaschke, F., Hietala, H., Angelopoulos, V., & Nakamura, R. (2016). Geoeffective jets impacting the magnetopause are very common. *Journal of Geophysical Research: Space Physics*, *121*(4), 3240–3253. https://doi.org/10.1002/2016JA022534

Plaschke, F., Hietala, H., & Vörös, Z. (2020). Scale sizes of magnetosheath jets. *Journal of Geophysical Research: Space Physics*, *125*(9), e2020JA027962. https://doi.org/10.1029/2020JA027962

Plaschke, F., Hietala, H., Archer, M., Blanco-Cano, X., Kajdič, P., Karlsson, T., et al. (2018). Jets downstream of collisionless shocks. *Space Science Reviews*, *214*(5), 81. https://doi.org/10.1007/s11214-018-0516-3

Plaschke, F., Jernej, M., Hietala, H., & Vuorinen, L. (2020). On the alignment of velocity and magnetic fields within magnetosheath jets. *Annales Geophysicae*, *38*(2), 287–296. https://doi.org/10.5194/angeo-38-287-2020

Raptis, S., Karlsson, T., Plaschke, F., Kullen, A., & Lindqvist, P.-A. (2020). Classifying magnetosheath jets using MMS: Statistical properties. *Journal of Geophysical Research: Space Physics*, *125*(11), e2019JA027754. https://doi.org/10.1029/2019JA027754

Ross, S. (2013). Chapter 4—Generating discrete random variables. In S. Ross (Ed.), *Simulation* (5th ed., pp. 47–68). Academic Press. https://doi.org/10.1016/B978-0-12-415825-2.00004-8

Russell, C. T., Anderson, B. J., Baumjohann, W., Bromund, K. R., Dearborn, D., Fischer, D., et al. (2016). The magnetospheric multiscale magnetometers. *Space Science Reviews*, *199*(1), 189–256. https://doi.org/10.1007/s11214-014-0057-3

Schwartz, S. J. (1991). Magnetic field structures and related phenomena at quasi-parallel shocks. *Advances in Space Research*, *11*(9), 231–240. https://doi.org/10.1016/0273-1177(91)90039-M

Shue, J.-H., Song, P., Russell, C. T., Steinberg, J. T., Chao, J. K., Zastenker, G., et al. (1998). Magnetopause location under extreme solar wind conditions. *Journal of Geophysical Research: Space Physics*, *103*(A8), 17691–17700. https://doi.org/10.1029/98JA01103

Spreiter, J. R., Summers, A. L., & Alksne, A. Y. (1966). Hydromagnetic flow around the magnetosphere. *Planetary and Space Science*, *14*(3), 223–253. https://doi.org/10.1016/0032-0633(66)90124-3

Suvorova, A. V., & Dmitriev, A. V. (2015). Magnetopause inflation under radial IMF: Comparison of models. *Earth and Space Science*, *2*(4), 107–114. https://doi.org/10.1002/2014EA000084

Suvorova, A. V., & Dmitriev, A. V. (2016). On magnetopause inflation under radial IMF. *Advances in Space Research*, *58*(2), 249–256. (Plasma Transport Across Magnetospheric Boundaries). https://doi.org/10.1016/j.asr.2015.07.044

Suvorova, A. V., Shue, J.-H., Dmitriev, A. V., Sibeck, D. G., McFadden, J. P., Hasegawa, H., et al. (2010). Magnetopause expansions for quasi-radial interplanetary magnetic field: THEMIS and Geotail observations. *Journal of Geophysical Research*, *115*(A10). https://doi.org/10.1029/2010JA015404

Vuorinen, L., Hietala, H., & Plaschke, F. (2019). Jets in the magnetosheath: IMF control of where they occur. *Annales Geophysicae*, *37*(4), 689–697. https://doi.org/10.5194/angeo-37-689-2019

Wang, B., Nishimura, Y., Hietala, H., Lyons, L., Angelopoulos, V., Plaschke, F., et al. (2018). Impacts of magnetosheath high-speed jets on the magnetosphere and ionosphere measured by optical imaging and satellite observations. *Journal of Geophysical Research: Space Physics*, *123*(6), 4879–4894. https://doi.org/10.1029/2017JA024954

Zhang, T., Zhao, H., Russell, C., Petrinec, S., Schwingenschun, K., & Riedler, W. (1997). Dayside reconnection during IMF northward: A possible foreshock effect. *Advances in Space Research*, *19*(12), 1943–1946. (Proceedings of the D0.4 Symposium of COSPAR Scientific Commission D). https://doi.org/10.1016/S0273-1177(97)00106-3